

# Optic flow instructs retinotopic map formation through a spatial to temporal to spatial transformation of visual information

Masaki Hiramoto and Hollis T. Cline<sup>1</sup>

Department of Molecular and Cellular Neuroscience, Dorris Neuroscience Center, The Scripps Research Institute, La Jolla, CA 92037

Edited by Carla J. Shatz, Stanford University, Stanford, CA, and approved October 15, 2014 (received for review September 2, 2014)

**Retinotopic maps are plastic in response to changes in sensory input; however, the experience-dependent instructive cues that organize retinotopy are unclear. In animals with forward-directed locomotion, the predominant anterior to posterior optic flow activates retinal ganglion cells in a stereotyped temporal to nasal sequence. Here we imaged retinotectal axon arbor location and structural plasticity to assess map refinement in vivo while exposing *Xenopus* tadpoles to visual stimuli. We show that the temporal sequence of retinal activity driven by natural optic flow organizes retinotopy by regulating axon arbor branch dynamics, whereas the opposite sequence of retinal activity prevents map refinement. Our study demonstrates that a spatial to temporal to spatial transformation of visual information controls experience-dependent topographic map plasticity. This organizational principle is likely to apply to other sensory modalities and projections in the brain.**

temporal code | topographic map | activity-dependent plasticity | STDP | visual system

In the visual system, the sensory world is mapped onto the planar array of retinal ganglion cells (RGCs), and this representation of the visual world is then conveyed to the CNS via the spatial distribution of retinal axons in the target area. It is widely accepted that molecular cues guide retinal axons to approximate regions along the rostrocaudal axis of the target and that activity-dependent mechanisms refine this crude map (1–3). Moreover, retinotopic maps show experience-dependent plasticity throughout life, allowing them to accommodate changes in the sensory periphery as well as the brain. Current models of activity-dependent mechanisms of topographic map plasticity are based on coactivity rules (4–7), however information in natural scenes may be encoded in additional temporal properties of neuronal firing other than coactivity (8–11). For instance, temporal features of RGC spiking have been shown to encode information about the visual stimuli (12). Movement of objects through the visual field activates RGCs in a temporal sequence, which corresponds to a progression of spatial locations of the object in the visual scene. This raises the possibility that the temporal sequence of RGC activity might encode spatial information that can be used to organize retinotopic maps.

A candidate visual input that shapes retinotopy is optic flow. In most forward-moving animals, the direction of optic flow is biased from anterior to posterior (A→P). For instance, tadpoles always swim forward, and the predominant visual stimulus they experience is A→P motion within the visual scene. This generates an overall correlation between the sequential order of RGC activity from temporal to nasal retina and the retinotopic distribution of axon projections along the rostrocaudal axis of the tectal target (13). However, whether or how the relative sequence of activity induced by optic flow organizes retinotopy is unclear.

We tested whether the spatial arrangement of sensory afferents in the retinotopic map is encoded by the temporal sequence of RGC activity evoked by A→P moving visual stimuli. Starting in young tadpoles in which retinotectal inputs are highly overlapping and show no retinotopy, we used in vivo time-lapse im-

aging of retinotectal axon arbor positions to show that exposure to A→P motion stimulus produces an organized retinotopic map, whereas P→A motion stimulus produces poor retinotopy. These data suggest that sequential activation of RGCs along the temporal to nasal retinal axis provides information that is critical for organizing retinotopy. To gain more precise control over the relative timing of convergent retinal inputs, we used tadpoles with induced binocular input to the tectum, and we sequentially stimulated the left and right eyes at interstimulus intervals from 15 to 100 ms. In vivo time-lapse imaging showed that the relative timing of activity in convergent retinotectal inputs specifies axon position along the rostrocaudal tectal axis: Axons stimulated 15–50 ms earlier than convergent inputs from the other eye shift their positions to terminate in relatively more rostral tectal positions than the later stimulated axons. This study indicates that the reliable temporal to nasal sequence of RGC activity induced by predominant forward locomotion provides a temporal code that is transformed into the spatial order of axon projections of RGCs. Furthermore, analysis of branch dynamics demonstrates that the plasticity mechanism operated by regulating the location of branch retractions within the arbor. We propose that the transformation of a temporal sequence of input activity into the spatial organization of afferents in the retinotopic map ensures the development and maintenance of a retinotopic projection scaled across the available target space.

## Results

**Retinotopic Map Refinement Is Regulated by the Direction of Moving Visual Stimuli.** Natural A→P optic flow in free-swimming tadpoles activates RGCs sequentially from temporal to nasal retina (Fig. 1A).

### Significance

**Topographic maps of the sensory world are distributed throughout the brain. Maps are important because they facilitate information transfer within and between brain regions. We know that sensory experience is required for the development and plasticity of sensory maps, but the elements of natural sensory experience that instruct map formation have not been identified. Here we show that natural optic flow produces a temporal code of retinal activity that instructs the spatial organization of retinotopic maps. Our study demonstrates that visual information is transformed from a temporal code to a spatial code in the brain. Such transformations of information codes are likely to occur throughout the brain.**

Author contributions: M.H. and H.T.C. designed research; M.H. performed research; M.H. analyzed data; and M.H. and H.T.C. wrote the paper.

The authors declare no conflict of interest.

This article is a PNAS Direct Submission.

Freely available online through the PNAS open access option.

<sup>1</sup>To whom correspondence should be addressed. Email: cline@scripps.edu.

This article contains supporting information online at [www.pnas.org/lookup/suppl/doi:10.1073/pnas.1416953111/-DCSupplemental](http://www.pnas.org/lookup/suppl/doi:10.1073/pnas.1416953111/-DCSupplemental).

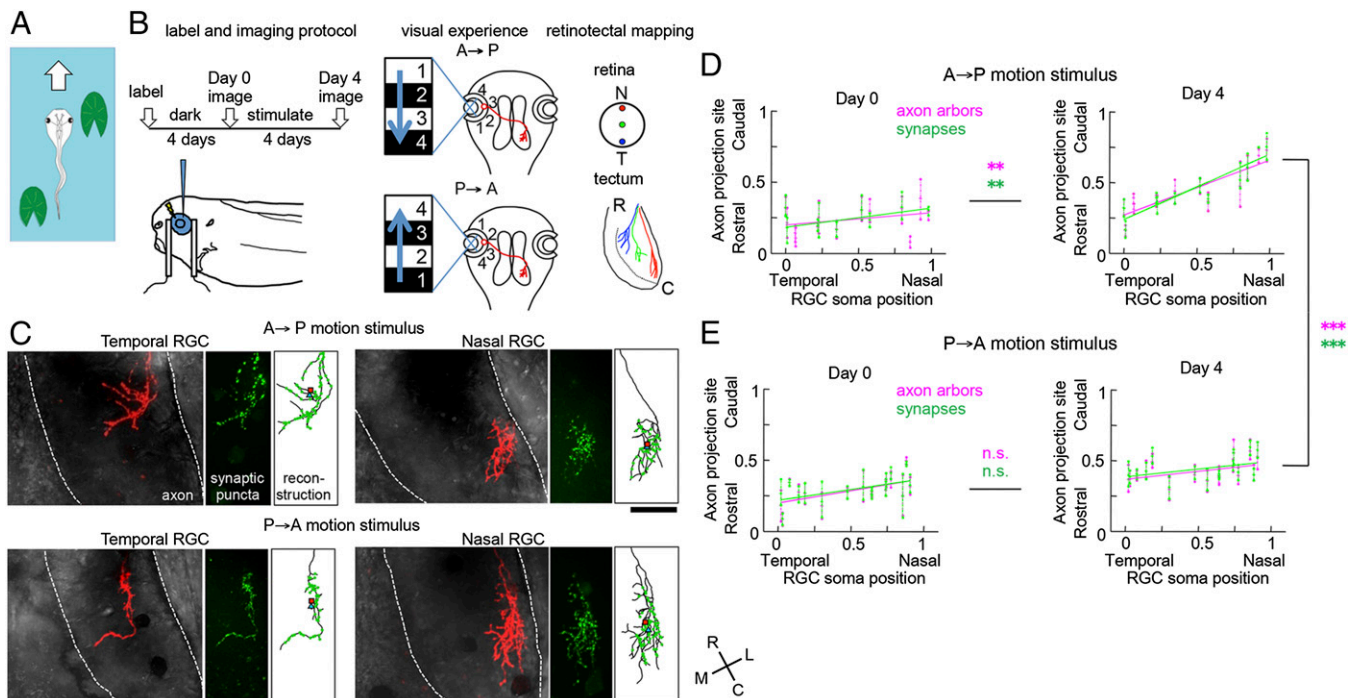


**Fig. 1.** Retinotopic map refinement is regulated by the direction of optic flow. (A) Tadpoles swim forward, so they experience a predominant A→P optic flow. (B) Schematic of experimental protocol. RGCs were labeled with TdTomato and Syn-GFP (Bottom Left). Animals were exposed to A→P or P→A moving stimuli for 10 h/d for 4 d. Retinotectal axons were imaged before and after visual stimulation. Positions of labeled RGC somata and axon arbors were determined. N and T mark the nasal and temporal retina; R and C mark the rostral and caudal tectum. (C) Representative images of axon arbors collected after 4 d of A→P (Top) or P→A (Bottom) motion stimulus superimposed on a DIC image of the tectum (Left). (Middle) Images of Syn-GFP puncta. (Right) Reconstructions of axons (black lines) showing puncta (green) and centers of mass for axons (red squares) and synapses (blue triangles). Positions of somata as percentiles along the temporo-nasal axis are 0, 87 (A→P), and 2, 88 (P→A) (from Left to Right). (Scale bar, 100  $\mu\text{m}$ .) (D and E) Topographic maps before and after 4 d of A→P or P→A visual motion stimulus. Relative positions of RGC somata along the temporo-nasal retinal axis and the centers of mass of the retinotectal axon arbors (magenta) and Syn-GFP puncta (green) along the rostrocaudal tectal axis are mapped. Bars indicate 25th and 75th percentiles of the distribution of axon branches along the rostrocaudal tectal axis. Before visual experience, soma positions and axon projection sites are not significantly correlated (D, axon arbors,  $R = 0.34$ ,  $P > 0.2$ ; synapses,  $R = 0.56$ ,  $P > 0.09$ ) or weakly correlated (E, axon arbors,  $R = 0.61$ ,  $P = 0.013$ ; synapses,  $R = 0.57$ ,  $P = 0.022$ ). Somata positions and axon projection sites were clearly correlated after 4 d of A→P motion stimulus (D, axon arbors,  $R = 0.89$ ,  $P < 0.001$ ; synapses,  $R > 0.9$ ,  $P < 0.001$ ), but not after 4 d of exposure to P→A stimulus (E, axon arbors,  $R = 0.45$ ,  $P = 0.066$ ; synapses,  $R = 0.43$ ,  $P = 0.094$ ). Retinotopy was sharpened after 4 d of A→P stimulus, not after P→A stimulus [ANCOVA (day 0, day 4), A→P,  $***P < 0.01$  (axons, synapses),  $n = 13$  (axons) and 11 (synapses); P→A,  $P > 0.4$  (axons),  $P > 0.6$  (synapses),  $n = 13$ ]. Retinotopy was significantly different after 4 d of A→P and P→A stimulus [ANCOVA (A→P, P→A),  $***P < 0.001$ ,  $n = 13$  (A→P, synapse, 11) and 16 (P→A)], not before the stimulation [ $P > 0.3$  (axons) and  $P = 0.9$  (synapses)]. The rostrocaudal extents of the arbors are not significantly different between A→P and P→A samples on day 4 ( $P = 0.36$ ).

To test whether the temporal sequence of RGC activity evoked by optic flow regulates the scaled topographic distribution of retinotectal axons along the rostrocaudal axis in the optic tectum, we evaluated retinotopy in tadpoles exposed to A→P or P→A motion stimulus. RGCs in young tadpoles (stage 41) were electroporated with plasmids encoding cytosolic tdTomato and Synaptophysin-GFP (Syn-GFP) to label axon arbors and presynaptic puncta, respectively. Tadpoles were kept in the dark until imaging experiments began 4 d later to prevent experience-dependent effects on visual circuit development. Images of single retinotectal axons, presynaptic boutons, and a differential interference contrast (DIC) image of the tectum were collected *in vivo*. Tadpoles were then divided into three groups and exposed to a visual stimulus of bars moving from A→P or P→A for 10 h/d for 4 d, or kept in the dark. The same retinotectal axons were imaged after the 4-d visual stimulation protocol (Fig. 1 B and C). Topographic maps were plotted as the positions of labeled RGC somata along the nasotemporal axis of the eye versus the positions of the center of mass of their retinotectal axons along the rostrocaudal axis of the tectum (Fig. 1 B, D, and E). The correlation of the RGC soma position to axon projection sites and the slope of the regression lines on the maps were used to quantify retinotopy. Flatter slopes indicate poor retinotopy, in which axons from temporal and

nasal RGCs overlap in similar tectal locations, and steeper slopes indicate more refined retinotopy. Time-lapse imaging showed that retinotopy was poor at day 0 and was selectively sharpened by 4 d of exposure to A→P visual motion stimulus, but not by P→A motion stimulus (Fig. 1 D and E) or dark-rearing (Fig. S1 A–D).

Tectal cells do not exhibit directional preference either in responsiveness or in training-induced plasticity (14), and optic nerve recordings showed no directional preference in the responses (Fig. S1E). Therefore, preferential responses of retinal or tectal neurons to A→P stimuli likely do not account for the selective effects of A→P stimuli on retinotopy. These results indicate that the direction of moving stimuli in the visual scene affects the refinement of retinotopic maps.

#### Temporal Control of Convergent RGC Activity in Binocular Tecta.

A→P moving bars activate RGCs sequentially from temporal to nasal retina. Therefore, temporal RGC axons, which innervate rostral tectum fire before sequentially more nasal RGC axons, innervate relatively more caudal positions in tectum. The observation that A→P stimuli preferentially organize the retinotopic map prompted us to investigate the hypothesis that the temporal to nasal sequence of retinotectal axon activity resulting

from A→P motion stimulus provides an instructive cue that directs the distribution of axon position along the rostrocaudal axis of the tectal neuropil. In particular, the hypothesis predicts that arbors of RGCs stimulated relatively earlier than convergent arbors shift their positions toward rostral tectum, whereas arbors of RGCs stimulated later shift their positions toward caudal tectum.

To test this hypothesis, we generated tadpoles with binocular retinotectal innervation, by ablating one tectal lobe. Because inputs from the two eyes are highly overlapping within the first weeks after tectal ablation (15, 16), this preparation provides an opportunity to gain precise temporal control over RGC activity by visually stimulating the two eyes independently (Fig. 2*A*). In normal tadpoles, light stimulus delivered to one eye resulted in RGC axon spiking in the optic nerve ipsilateral to the stimulated eye (Fig. 2*B, Top*) but not in the contralateral optic nerve (Fig. 2*B, Bottom*), indicating that visual stimuli applied to one eye do not activate the other eye. Similarly, visually evoked excitatory postsynaptic currents (EPSCs) could be recorded only from tectal cells contralateral to the stimulated eye in normal tadpoles (Fig. 2*C*). By contrast, tectal cells are binocular in animals with dually innervated tecta (Fig. 2*D*). When the left and right eyes were stimulated with a specific interstimulus interval, EPSCs with comparable intervals were recorded in the tectal neurons (Fig. 2*E*). To test whether spiking can be controlled reliably with our visual stimulation protocol, we measured first-spike latencies recorded from tectal cells with the cell attached mode following visual stimulation of the contralateral or ipsilateral eyes (Fig. 2*F*). More than 90% of first-spike latencies of individual trials

occurred within 10 ms of the mean latency (Fig. 2*G*). These data show that this preparation provides tight and reproducible temporal control over the activity of convergent axons in tectum.

**Temporal Sequence of RGC Activity Directs Retinotectal Arbor Position.** We then assayed whether axon arbors in binocular tecta shift their positions in response to simultaneous or sequential visual stimulation to the eyes. We labeled RGCs with tdTomato and Syn-GFP and collected an initial image of the retinotectal axon (day 0). Then tadpoles were placed in a chamber in which the left and right eyes were stimulated sequentially with light-emitting diodes (LEDs) at interstimulus intervals of 15, 50, or 100 ms every 11 s for 10 h/d for 2 d. Stimulation of the left and right eyes in this system mimics the relative sequence of activity in overlapping axon arbors in response to A→P stimuli in the normal circuit (Fig. 3*A, Top Left* and *Bottom Left*). When an axon arbor is stimulated earlier in the binocular circuit (Fig. 3*A, Top Right*), it corresponds to arbors from RGCs in more temporal retinal positions in normal animals with the A→P visual stimulation (Fig. 3*A, Top Left*). When an arbor is stimulated later (Fig. 3*A, Bottom Right*), it corresponds to arbors from RGCs in relatively more nasal retinal positions in normal animals with the A→P visual stimulation (Fig. 3*A, Bottom Left*). Axons were imaged each day after stimulation (Fig. 3*B–D*). Retinotectal axons gradually shift their retinotopic positions as a result of spatially biased distribution of changes in branch positions (3, 16, 17). To analyze movement of branches in response to visual stimulation, we aligned reconstructions of the axon arbors from time-lapse images and calculated the direction and magnitude of branch

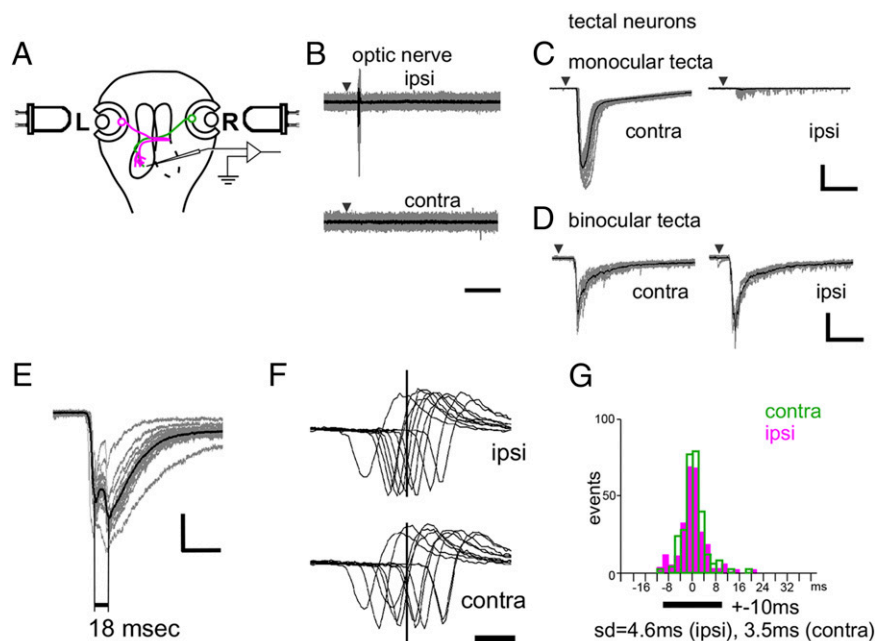


**Fig. 2.** Temporal control of activity in convergent inputs in binocular tecta. (A) Schematic of tadpoles with binocular tectal innervation. The right tectal lobe was ablated and both optic nerves crushed to produce highly overlapping retinotectal inputs from both eyes. Visual responses were recorded from tectal cells or optic nerves by stimulating left or right eyes with dimming light. (B) Light-evoked responses recorded in the optic nerves ipsilateral and contralateral to the stimulated eye. Focal LED stimulation to one eye only produces spikes in the optic nerve from the stimulated eye. (C) Visually evoked EPSCs recorded from tectal cells. In normal animals, monocular tectal cells only respond to stimuli applied to the contralateral eye. (D) Tectal cells in binocular tecta respond to stimuli applied to either eye, contralateral or ipsilateral to the optic tectum from which recordings were made, indicating that tectal cells receive binocular inputs. The amplitudes of EPSCs evoked by visual stimulation of the ipsilateral and contralateral eyes were not significantly different [ $P = 0.32$ ,  $n = 7$ ; Mann-Whitney, peak currents (mean  $\pm$  SEM) ipsilateral,  $-81.7 \pm 11.6$  pA; contralateral,  $-102 \pm 12.4$  pA]. (E) When eyes contralateral and ipsilateral to the binocular tectum are stimulated with an interval of 20 ms, tectal cell EPSCs exhibit two peaks matching the stimulus interval. (F and G) Analysis of variance of first-spike latencies. (F) Recordings of 10 visually evoked spikes in a binocular tectal cell in response to visual stimuli to the eye ipsilateral or contralateral to the tectum. The vertical line shows the mean first-spike latency for the two inputs. (G) Histogram of first-spike latencies relative to the mean latency. Ninety percent of first-spike latencies occur within 10 ms of the mean latency.  $n = 267$  (ipsi) and 270 (contra) spikes from 13 cells. Sweeps of 20 (B–E) trials, shown in gray, are overlaid with the average, shown in black. [Scale bar, 200 ms (B–D), 50 ms (E), 5 ms (F), 200 pA (C), and 100 pA (D and E).]



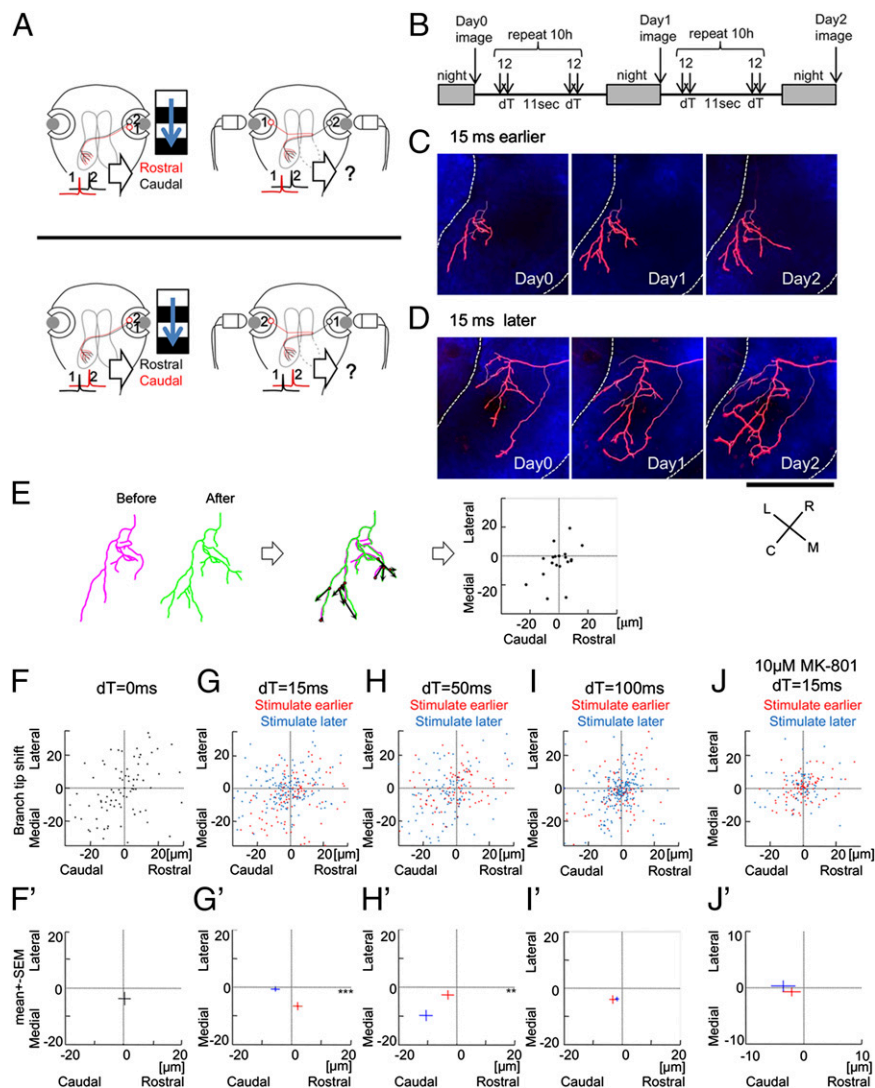


**Fig. 3.** The temporal sequence of activity in convergent inputs directs topographic shifts in axon arbor position. (A) Schematics showing the relation between A→P motion stimulus in normal tadpoles (Left) and sequential stimulation of the eyes in animals with binocular tecta (Right). The positions of RGCs that were labeled and imaged are shown in red. Numbers 1 and 2 correspond to the sequence of stimulation of the RGCs (Left) or eyes (Right). (Left) In normal tadpoles, the sequential order of activity in overlapping axon arbors induced by A→P stimulus specifies arbor position. For two neighboring RGCs, numbered 1 and 2, when the labeled arbor from the temporal RGC (red, Top) is activated before the arbor from a neighboring RGC positioned more nasally with the retina (black), in vivo imaging shows that the earlier-stimulated arbor from the temporal RGC will eventually be located more rostrally than the later-activated arbor from the nasal RGC. When the nasal RGC is labeled (red, Bottom), it is the later-stimulated axon with the A→P motion stimulus—that is, RGC 2—and it will be located more caudally in the tectum than the earlier activated arbor from temporal retina. (Right) In tadpoles with binocular tecta, stimulating the labeled (red) left eye earlier (1, Top Right) or later (2, Bottom Right) than the unlabeled right eye (black) mimics the sequential order of activity with A→P optic flow in which temporal RGCs are activated earlier than nasal RGCs. (B) Schematic of experimental protocol. Images are collected once a day. Eyes are stimulated with a 15-ms interstimulus interval once every 11 s for 10 h/d. (C and D) Images of representative axons from animals in which eyes were stimulated sequentially with a 15-ms interstimuli interval. The eye with the labeled axon was stimulated earlier (C) or later (D) than the other eye. (Scale bar, 100  $\mu\text{m}$ .) The axes under D show the orientation of the images and drawings in C–E. C, caudal; L, lateral; M, medial; R, rostral. (E) Alignment of images shown in C, based on the iterative closest point algorithm used to calculate changes in branch tip positions (magenta, day 0; green, day 1). Established axon branches are stable within the optic tectum over the imaging period (17) (Fig. S2A), enabling alignment of time-lapse arbor images. Changes in branch tip positions were calculated by subtracting the vectors from branch points to the branch tips for each branch at sequential time points (Middle, black arrows) and displayed on a Cartesian coordinate (Right). (F–J) Plots of the movement in branch tip positions for earlier-stimulated and later-stimulated arbors (red and blue data points, respectively). Each data point indicates the shift of individual axon branches. Lower panels show mean  $\pm$  SEM of the shift in branch tip positions (see Table S1 for values). The branch displacements are significantly different between the earlier- and later-stimulated conditions for interstimulus intervals of 15 and 50 ms (G–H') but not for 100 ms (I and I'). MK801 (10  $\mu\text{M}$ ) eliminated the difference in branch tip shift normally seen when the eyes are stimulated with 15-ms interstimuli intervals (J and J'). \*\* $P < 0.01$ , \*\*\* $P < 0.001$  (see Table S1 for values).

tip movements over the 2 d. A Wald–Wolfowitz runs test indicates that the directions of movements of branches within individual arbors are independent of one another (Table S2). The movement of each branch tip was plotted on a coordinate map of the tectum, where the center (0, 0) represents the branch

tip position at the first image (Fig. 3E). Branch tips that do not move over the imaging interval are plotted at the center (0, 0). Those that move rostrally or caudally are plotted to the right and left of center, respectively, and those that move medially or laterally are plotted to the left and right of center, respectively. Stimulating

the eyes sequentially with interstimulus intervals of 15 and 50 ms resulted in significant differences in branch tip movements along the rostrocaudal tectal axis that were not seen with the 100-ms interstimulus interval (Fig. 3 *G–I* and *G'–I'* and Fig. S2 *B* and *C*). Branch tip movements were scattered along the mediolateral axis, but did not shift consistently with the different stimulus conditions. Retinotectal axons from the eye that was stimulated earlier than the other eye shifted toward rostral tectum, and those that were stimulated later than the other eye shifted toward caudal tectum for the 15-ms interstimulus interval. The mean displacements in branch tip positions for earlier- and later-stimulated axons over 2 d were 7.5  $\mu\text{m}$  and 8  $\mu\text{m}$  for interstimulus intervals of 15 and 50 ms, which corresponds to about 11–12% of the average rostrocaudal length of the arbors. This also corresponds to about 16% of the maximal displacement of nasal axons toward caudal tectum seen after 4 d of exposure to A→P motion stimuli (Fig. 1*D* and Fig. S1*C*). Axon arbor branch lengths and growth rates were not different between the different groups (Fig. S3 *A–E*). Analysis of the distribution of synaptic puncta in retinotectal axons indicate that dynamic branches form synapses with tectal neurons and suggest that synaptic mechanisms can contribute to a shift of retinotectal axon arbors in the tectum (Fig. S4). Exposing animals to the use-dependent N-methyl-D-aspartate receptor

(NMDAR) antagonist MK801 (10  $\mu\text{M}$ ), starting 12 h before and continuing through the visual stimulation period, blocked the shift in branch tip positions seen in control animals (Fig. 3 *J* and *J'*). These data indicate that axon arbor branches shift their topographic positions in the tectal neuropil in response to the temporal sequence of afferent activity by an NMDAR-dependent mechanism. The optimal temporal interval to produce directional shifts in branch tip positions is 15–50 ms.

We then investigated whether changing the sequence of eye stimulation could reverse the direction that individual axons shift in tectum. Labeled retinotectal axons innervating binocular tecta were imaged at days 0, 1, and 2. Between the first and second images, we stimulated the eyes sequentially with an interstimulus interval of 20 ms every 11 s for 10 h/d. The next day we reversed the order of eye stimulation, and a third image of the axon was collected after 10 h of stimulation (Fig. 4*A*). We compared the effects of sequential stimuli with simultaneous stimulation of the two eyes ( $dT = 0$  ms), which does not mimic the sequential order of RGC activation by the motion stimulus. Images of axon arbors from animals that received sequential or simultaneous eye stimulation are shown in Fig. 4 *B* and *C*. Superimposing individual images in the series from a representative animal illustrates the shift of arbor position when the eyes are stimulated sequentially (Fig. 4*B*,

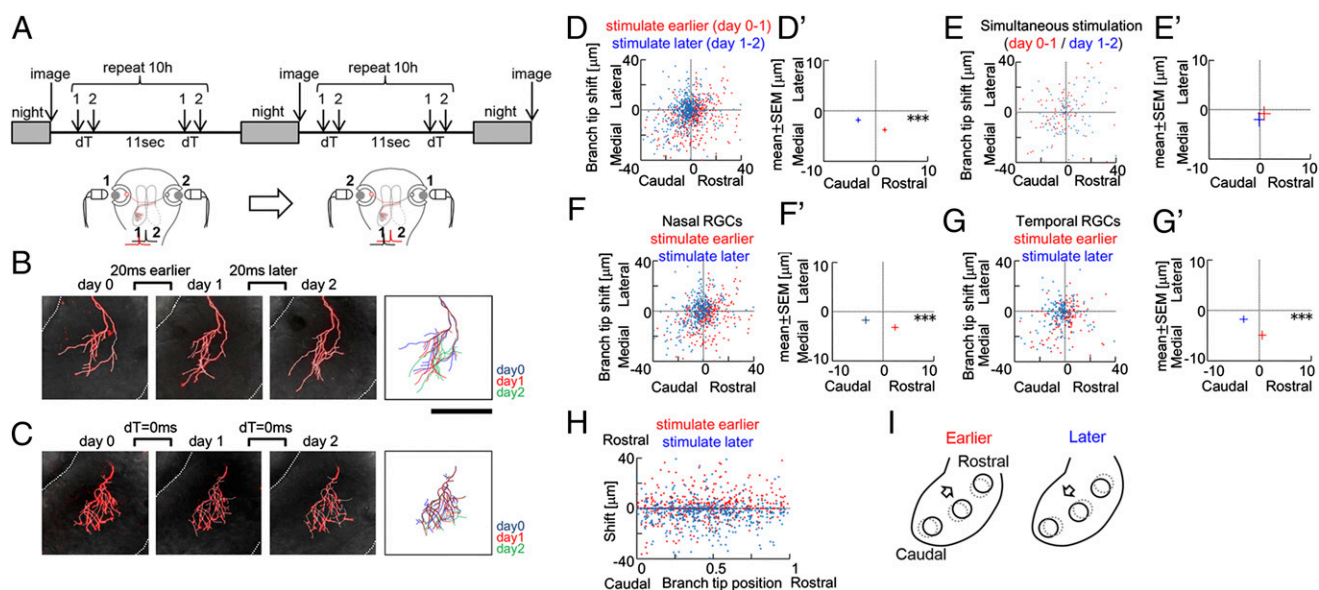


**Fig. 4.** The temporal sequence of input activity regulates the direction of branch tip movements. (*A*) Schematic of experimental protocol. The left and right eyes were stimulated simultaneously ( $dT = 0$  ms) or sequentially with an interstimulus interval of 20 ms ( $dT = 20$  ms) at 0.09 Hz for 10 h/d. The sequence of eye stimulation was reversed after the first day of stimulation. Cartoons of tadpoles show that the left eye with the labeled axon (red) was stimulated earlier (1, left cartoon) than the unlabeled right eye (black) during the first day of stimulation, and then the sequence of eye stimulation was switched so the left eye with the labeled axon was stimulated later (2, right cartoon) than the right eye. Images were collected daily before stimulation, as marked with arrows. (*B* and *C*) Images of representative axons from animals in which eyes were stimulated sequentially (*B*) or simultaneously (*C*). (*B*) Between the first 2 d, the eye with the labeled axon was stimulated 20 ms earlier than the other eye. The next day the order of eye stimulation was reversed. Superimposed axon reconstructions (*Right* panels in *B* and *C*) show axon rearrangements with sequential eye stimulation. (Scale bar, 100  $\mu\text{m}$ .) (*D* and *E'*) Plots (*Top*) of shifts in branch tip positions in axons from animals stimulated with  $dT = 20$  ms (*D* and *D'*) or  $dT = 0$  ms (*E* and *E'*). Shifts in branch tip positions when the labeled axon was stimulated earlier (red) or later (blue) than convergent inputs from the other eye. (*D'* and *E'*) Summary plots (*Bottom*) of the mean and SEM of the shift in branch tip position (see Table S3 for values). SEM is shown as the length of the bars in the symbols. The displacements in branch tip positions were significantly different between the two periods when the eyes were stimulated sequentially ( $P < 0.001$ , paired *t* test,  $n = 612$  from 16 axons) but not with simultaneous stimulation ( $P = 0.6$ , paired *t* test,  $n = 167$  from eight axons). Effect sizes (*d*), which are independent of sample size, were also different between  $dT = 20$  ms (0.4) and  $dT = 0$  ms (0.06). (*F* and *G'*) Plots (*Top*) of the shifts in branch tip positions in axons from RGCs from the nasal (*F* and *F'*) and temporal (*G* and *G'*) halves of retina. Summary plots (*Bottom*) show the mean and SEM of the shift in branch tip position. Similar shifts in branch tip positions were observed for both groups (temporal RGCs,  $P < 0.001$ , 207 branches; nasal RGCs,  $P < 0.001$ , 405 branches; Table S3). (*H*) Plot of the magnitude of branch tip shift along the rostrocaudal axis relative to the initial branch tip position for axons stimulated 20 ms earlier (red) or later (blue) than inputs from the other eye. The branch tip movements toward rostral or caudal tectum in response to the temporal order of stimulation were observed along the rostrocaudal extent of the tectum. See Fig. S5 for further analysis of branch movements. (*I*) Schematic of observations. Axon arbors that are consistently stimulated earlier than converging inputs shift rostrally (*Left*). Conversely, axon arbors that are consistently stimulated later than converging inputs shift caudally (*Right*). \*\*\* $P < 0.001$ .

Right) compared with the relative stability of arbor position when the eyes are stimulated simultaneously (Fig. 4C, Right).

Axons changed the direction of movement of their branch tips over a 10-h period when the temporal sequence of visual stimulation was reversed. When the eye with the labeled axon was stimulated 20 ms before the other eye, the axon branch tips moved to more rostral tectal positions (Fig. 4D and D', red and Fig. S5A and C, red), and when the order of eye stimulation was reversed the following day, the same axon extended branches toward caudal tectum (Fig. 4D and D', blue and Fig. S5A and C, blue). Axon branch movements were not significantly different between the two imaging intervals when both eyes were stimulated simultaneously (Fig. 4E and E' and Fig. S5B and D). Branch tip shifts are comparable in RGC axons from nasal and temporal halves of retina (Fig. 4F, F', G, and G') and in axons from eyes ipsilateral or contralateral to the binocular tectum (Fig. S6). Shifts in branch tip positions are distributed along the rostrocaudal tectal axis (Fig. 4H). The mean shift in branch tip

position is 6  $\mu\text{m}/\text{d}$ , which corresponds to about 9% of the average rostrocaudal length of the arbors. Axon arbor branch lengths and growth rates over the two periods were not significantly different (Fig. S3F–J).

**Temporal Sequence of Input Activity Regulates the Distribution of Dynamic Branches.** The results above suggest that the temporal sequence of input activity shifts axon arbor branch positions. Dynamic branch additions and retractions contribute to the net shift in axon arbors (3, 16–24). Furthermore, a recent study indicates that asynchronous stimulation of retinal inputs induces branch dynamics (7). We next analyzed axon branch dynamics in arbors imaged at daily intervals over 3 d with a 15-ms interstimulus interval to compare the spatial distribution of dynamic branches in arbors stimulated earlier or later than convergent inputs (Fig. 5A). Dynamic branches were categorized as added, transient, and lost, as shown in Fig. 5B and C. Unstable branches include both lost and transient branches. We

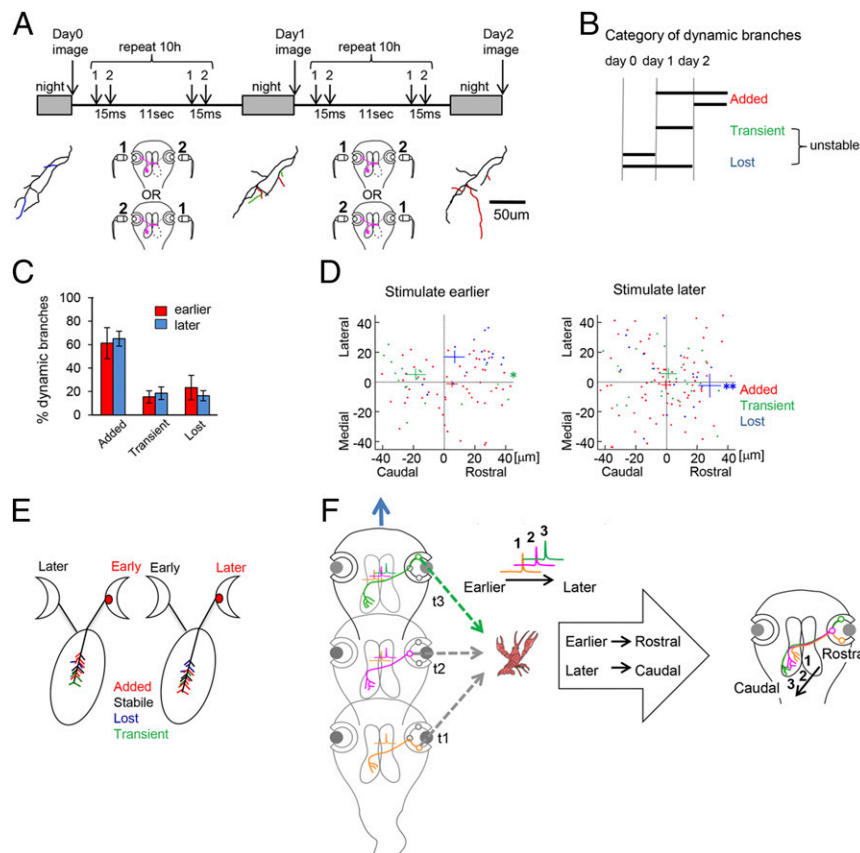


**Fig. 5.** The temporal sequence of input activity regulates the spatial distribution of dynamic branches. (A) Schematic of experimental protocol. Arbors were imaged once a day. Animals received sequential eye stimulation ( $dT = 15$  ms) for 10 h/d for 2 d. "1," "2," order of stimulation. (B) Schematic analysis of branch dynamics. The morphology of axons imaged at different time points is compared to identify and classify dynamic branches. "Added" branches (red) emerged during the imaging session and were maintained to the last image. "Transient" branches (green) emerged and were subsequently lost during the imaging period. "Lost" branches (blue) were present at the first image and were retracted during the imaging period. (C) Percentage of each dynamic branch category for earlier- and later-stimulated axons. (D) Shift in spatial distributions of dynamic branches in axons stimulated 15 ms earlier (Left) or later (Right) than convergent inputs from the other eye. The plots show the positions of the added, transient, and lost branches relative to the center of gravity of all new (added + transient) branches. In earlier-stimulated axons, transient branches were located caudal to the mean of new branches ( $P = 0.012$ ,  $n = 102$  branches, seven axons). In later-stimulated axons, lost branches are located rostral to the mean of new branches ( $P < 0.001$ ,  $n = 146$  branches, seven axons). (E) Schematic of observations. The centers of mass of the earlier- and later-stimulated arbors displaced toward the rostral and caudal tectum, respectively, because of the different distributions of unstable branches. In earlier-stimulated axons, transient branches retracted in the caudal region of the arbor, and in later-stimulated axons, branches retracted from the rostral region of the arbor. (F) Schematic of the mechanism in which optic flow provides an antero-posterior cue to refine retinotopy. (Left) With forward motion of the animal, an image projected from an object stimulates RGCs in a reproducible temporal to nasal sequence ( $t_1$ ,  $t_2$ ,  $t_3$ ), resulting in the sequential activation of RGC axons (labeled 1, 2, 3). (Middle) The plasticity rule described here instructs axons to project along the rostrocaudal tectal axis based on the sequence of activity according to a fixed relationship where earlier-activated axons are directed to correspondingly more rostral locations in tectum compared to later-activated axons. (Right) This rule distributes axons along the rostrocaudal tectal axis.



mapped the locations of all dynamic branches in each arbor and plotted the distribution of transient, added, and lost branches relative to the center of mass of all added branches for each arbor (Fig. 5D). In arbors that were stimulated earlier than convergent inputs from the other eye, transient branches were located caudal to the mean of all new branches (Fig. 5D, Left, green cross). In axons that were stimulated later than inputs from the other eye, lost branches were located rostral to the mean of all new branches (Fig. 5D, Right, blue cross). Together, these branch dynamics produce a net displacement between earlier-stimulated arbors and later-stimulated arbors. Axons from the earlier- and later-stimulated conditions had comparable proportions of stabilized, transient, and lost branches (Fig. 5C). Therefore, it is unlikely that the differences in the spatial distributions of dynamic branches were caused by overall differences in the capacity for structural plasticity in the arbors. This analysis demonstrated a spatial bias in the distribution of unstable branches within the arbor, which results in a displacement in arbor position toward the rostral tectum in earlier-stimulated RGCs or toward the caudal tectum in later-stimulated RGCs (Fig. 5E). Analysis of branch dynamics in arbors imaged every hour over 4 h revealed no significant difference in the spatial distribution of transient and stable branches in earlier- or later-stimulated axons (Fig. S7), although experience-dependent modification in branch stability can be seen over short time scales (7, 16, 22, 24–26). The data support a model in which the predominant A→P motion stimulus resulting from natural optic flow produces a reproducible sequence of RGC activity along the temporal to nasal axis of the retina, and the temporal sequence of input activity instructs the spatial distribution of retinotectal axons along the rostrocaudal axis of the tectal neuropil.

## Discussion

Our results demonstrate that the spatiotemporal information provided by optic flow is encoded into the temporal sequence of activity in neighboring RGCs, which in turn is transformed into the spatial distribution of RGC arbors in the tectal retinotopic map (Fig. 5F). The predominant optic flow that tadpoles experience is from A→P within the visual scene, which produces a temporal to nasal sequence of activity in RGC somata. We demonstrate that persistent A→P visual motion stimulus promotes the refinement of a scaled distribution of axons along the rostrocaudal axis of the retinotopic map by regulating the spatial order of axon projections, whereas P→A visual motion stimulus results in poor retinotopy. By providing pairs of stimuli sequentially to the left and right eyes in tadpoles with binocular tectal input, we show that the temporal sequence of activity in retinal inputs determines the spatial arrangement of retinotectal axons along the rostrocaudal tectal axis. Specifically, we show that retinotectal axons whose activity precedes that of convergent axons from the other eye shift their positions toward rostral tectum, whereas axons whose activity is relatively delayed shift their positions toward caudal tectum. This mechanism explains how A→P visual motion stimulus selectively organizes retinotopy.

Previous studies in *Xenopus* tectum (14) and other circuits (27) have shown that brief training protocols with unidirectional motion stimulus induce a rapid and transient shift in visual receptive fields toward the direction of stimulus in the visual scene through spike-timing-dependent plasticity (STDP). Unlike the selective sharpening of retinotopy by A→P visual motion observed here, STDP shifts receptive fields in response to any direction of motion stimulus used in the training protocol. The acute displacement in visual receptive fields is thought to decrease reaction times by predicting the location of objects moving in a consistent direction (28, 29). The mechanism observed here may function homeostatically to ensure that proportionately scaled retinotopic projections are maintained over longer time spans despite repeated short-term modifications of neuro-

nal response properties. Importantly this mechanism is flexible and in principle can accommodate changes in peripheral or central structures by reorganizing the projection according to an updated temporal sequence of input activity (30–33).

The dually innervated tadpole retinotectal system has been used extensively to investigate mechanisms of eye-specific segregation and has provided valuable insight into the contributions of activity-dependent and activity-independent mechanisms in organizing visual projections (7, 16, 19, 21, 34–39). Here we used this system to gain temporal control over activity in convergent retinotectal axons before segregation of eye-specific inputs. Electrophysiological recordings from binocular tectal cells demonstrated that they resolve synaptic inputs from the left and right eyes stimulated sequentially with a 15-ms interval. We took advantage of the millisecond temporal control over visual input activity and in vivo time-lapse imaging of experience-dependent structural plasticity to test whether the temporal sequence of afferent activity governs the relative position of retinotectal axons in the tectum.

Studies in several systems indicate that synapse and branch dynamics underlie experience-dependent plasticity in organized sensory projections (3, 16, 24, 40–45). Here we show that the transformation of temporal information in retinotectal axon activity into spatial information of arbor position in the topographic map requires structural rearrangements of axon arbor morphology and retinotectal synaptic connections. We first analyzed shifts in retinotectal axon arbor position by determining the changes in individual axon branch tip positions over the period of visual experience. This measure incorporates branch retractions and branch extensions, as they both result in changes in branch tip positions. Changes in individual branch tip positions range from 0 to 40  $\mu\text{m}$ , whether the eyes are stimulated synchronously or sequentially, which is indicative of the capacity for structural rearrangements in the arbors. The mean shifts in branch tip positions seen in earlier- and later-stimulated axons are consistent with the idea that the temporal order of activity in retinotectal axons shifts the position of the arbor relative to other convergent inputs. Shifts in arbor positions can result from changes in a subset of branch tips. Because the mean changes in branch tip positions are calculated from all of the branches within the arbors, including those that appear stable over the observation period, they may underestimate changes in arbor position in the tectum.

Our subsequent analysis focused on the spatial distribution of dynamic branches and provided additional insight into the mechanism by which the temporal sequence of afferent activity results in structural changes in arbor position. We find that branch additions are widely distributed over the arbor area and that the directional shift in arbor position occurs as a result of spatial distribution in branch retractions. In arbors that are stimulated earlier than convergent inputs from the other eye, the net rostral shift in axon branches occurs as a result of the preponderance of transient branches in the caudal region of the arbor. In arbors that are stimulated later than convergent inputs from the other eye, the average location of lost branches in the rostral tectum accounts for the caudal shift in the arbor position. The shift in arbor position occurs gradually as a result of cumulative changes in the positions of branch additions and retractions, as reported in previous in vivo imaging studies (3, 16, 17, 20, 22, 24, 46, 47). These results indicate that the mechanism observed here directs retinotopic map refinement in response to the natural predominant A→P visual motion stimulus by activity-dependent mechanisms controlling axon branch and synapse lifetime.

In general, our data suggest that spatial information may be encoded in the temporal order of afferent activity and that the temporal order of afferent input activity can be decoded into a spatial representation of the inputs. Although anamniotes, such as tadpoles, use natural visual stimuli as the source of instructive

experience-dependent signals that refine retinotopic maps, comparable instructional cues in amniotes are provided by waves of activity that sweep across the retinas before vision (5, 48, 49). Recent work indicates that retinal waves in mammals are directionally biased from temporal to nasal retina (50, 51) similar to the activity evoked by optic flow with forward-directed locomotion, suggesting that the mechanism observed here may contribute to retinotopic map organization in amniotes. In addition to visual projections, afferents from whiskers (52) and lateral line organs are stimulated in a consistent sequence. Topographic projections are also present in nonsensory brain regions, including the hippocampus (53), where temporal sequences of activity encode memories (54, 55). In conclusion, we present evidence for a mechanism that translates temporal information in input activity into spatial representations of information in the brain. Such an organizational principle may operate to maintain order across and between multiple projections in the CNS.

## Methods

All experimental protocols were approved by The Scripps Research Institute Institutional Animal Care and Use Committee and complied with the guidelines established in the Public Health Service Guide for the Care and Use of Laboratory Animals.

**Tadpole Preparation.** Albino *Xenopus laevis* tadpoles were obtained either by matings of frogs from our colony, Nasco, or *Xenopus* Express Inc. All tadpoles were reared in an incubator at 22 °C with a 12 h light/12 h dark cycle until the experiments started. To analyze retinotopy, RGCs in stage 41 tadpoles were sparsely transfected with plasmids encoding tdTomato and Synaptophysin-GFP. Animals were anesthetized in 0.01% MS-222 solution and placed on an electrically grounded moist kimwipe. Two plasmids, pCMV:GAL4/UAS:tdTomato and pUAS:Synaptophysin-GFP (final concentrations, 0.5 µg/µL and 0.25 µg/µL, respectively), were mixed and pressure injected from a micropipette inserted between the retina and lens, using a picospritzer (Picospritzer II, General Valve Corporation). Fast Green (0.01%) was added to the DNA solution to monitor injection into the eye. The pipette tip was placed close to the center of the retina, and cells were electroporated by applying a single 37-V pulse of 1.6 ms. Animals were reared in the dark for 3 d until stage 45–46 and screened for successful labeling. For each experimental condition, ~1,000 animals were screened to identify those in which the soma position and the axon arbor position could be determined. Binocular tectal innervation was induced by ablating one tectal lobe (16), and the optic nerves were cut to synchronize retinal innervation of the remaining tectal lobe. For imaging experiments in dually innervated tecta, RGCs were sparsely labeled as described above, and the next day the tectal lobe contralateral to the labeled eye was ablated. Animals were screened 3 d after surgery to identify those with single-labeled retinotectal axons. Tadpoles were kept in the dark after tectal ablation until stage 48 to prevent visual experience-dependent effects on retinal axon arbors.

**Visual Stimulation Protocols.** For experiments with the moving bar stimulus, tadpoles were held in Sylgard chambers in transparent plastic containers and provided with a moving bar stimulus previously shown to induce plasticity of retinotectal responses (14). An liquid crystal display (LCD) displaying 10-mm-wide black stripes and 86-mm-wide white stripes (82 cd/cm<sup>2</sup>) moving at 78 mm/s (0.8 Hz) was placed 15 mm from the eyes. This corresponds to a speed of ~300 µm/s on the retina. The LCD display covers more than 120 degrees of the field of view. We presented the stimulus for 1 min with 5-min intervals for 10 h/d over 4 d. Animals were kept in the dark for the remaining 14 h/d.

For experiments in animals with dually innervated tecta, light (343 cd/m<sup>2</sup>) emitted from an LED (OptoSupply, OSHR5161A-QR, peak at 625 nm) was delivered to the eyes with a fiber optic. The beam was diffused with white silicon to reduce light that could indirectly stimulate the contralateral eye.

The stimulus was presented to both eyes synchronously or alternately to the left and right eyes at 0.09 Hz for 10 h/d. Some animals were treated with the NMDAR blocker MK801 (10 µM) in rearing solution throughout the stimulation protocol.

**Electrophysiology.** Stage 47/48 tadpoles were anesthetized in 0.02% MS222 and stabilized on Sylgard with dissecting pins. Electrophysiological recordings were taken from the optic nerve to monitor RGC responses to visual input, and from tectal neurons, using loose patch or whole-cell recordings, to determine postsynaptic responses to convergent retinal input. To record visually evoked field potentials, the skin over the tectum was removed, and an extracellular recording electrode, consisting of a glass micropipette filled with extracellular saline [115 mM NaCl, 4 mM KCl, 3 mM CaCl<sub>2</sub>, 3 mM MgCl<sub>2</sub>, 5 mM Hepes, 10 µM Glycine, 10 mM Glucose (pH 7.2)], was placed on the optic nerve. Visually evoked EPSCs in whole-cell mode or action potentials using loose patch recordings were recorded in animals as previously described (16). Recordings were performed with an Axopatch-200B amplifier and digitized using pClamp-8 software and a Digidata-1322A A/D-board (Axon Instruments). Animals were provided with visual stimulation to the eyes with a fiber optic as described above.

**In Vivo Time-Lapse Confocal Imaging and Analysis.** Confocal images of retinotectal axons, labeled with cytosolic tdTomato and Synaptophysin-GFP, were collected with a PerkinElmer Ultraview Vox spinning disk confocal mounted on a Nikon FN1 microscope with a 25×/N.A. 1.10 objective. For experiments with A→P and P→A moving bar stimulus, images were collected on the first, second, and sixth days before and after the visual stimulation sessions. The axon arbor morphology was reconstructed in the Filament tracing mode using IMARIS software. Branches longer than 2 µm were traced. To determine the center of mass of the arbors within the tectal neuropil, the neuropil was divided into 100 equal compartments along the rostrocaudal extent. The reconstructions of the axons were divided into 1-µm fragments, and the center of mass and 25th percentiles were calculated from the positions of the 1-µm fragments within the tectal compartments. For experiments in animals with dually innervated tecta, images were collected once a day over 4 d before and after the visual stimulation sessions. The axon arbor morphology was reconstructed using IMARIS software. For analysis of the shift in branch tip positions, the filament information was exported to MATLAB and analyzed. The traced filaments are aligned by an iterative closest point algorithm. Positional data from all corresponding branches were used for the alignment of the two axons. The shift of the branch tip position was calculated by subtracting the branch point to branch tip vectors before stimulation from the vector after the stimulation. The bias in the branch shift was analyzed by bootstrapping (1,000 repeats). Dynamic branches were categorized as added, transient, or lost. Added branches are branches that emerged and persisted to the end of the imaging period. Branches that were added and subsequently lost were categorized as transient. Lost branches were present initially and retracted completely during the imaging period. The spatial bias of the dynamic branches was analyzed by comparing the mean change in branch tip position with the center of mass of all added branches. The arbor size (Figs. 2 and 3) is measured as the rostrocaudal extent that covers 90% of the total length of branches at the second day.

To identify Synaptophysin-EGFP puncta, MATLAB programs for the following procedures were used. The 3D images of Synaptophysin-EGFP were processed by a filter that averages over 2 µm voxels. A background intensity value, determined as two SDs above the average intensity of the entire image, was subtracted from the image. The intensity of the Synaptophysin-EGFP signal was determined by scanning along the traced filament. Puncta were identified by a 10% rise and fall in intensity within 4 µm.

**ACKNOWLEDGMENTS.** We thank Drs. Anton Maximov and Edward Giniger, and members of the H.T.C. laboratory for helpful discussions. The work was supported by National Institutes of Health Grants EY011261 and DP10D000458, the Nancy Lurie Marks Family Foundation, and an endowment from the Hahn Family Foundation (to H.T.C.).

- Feldheim DA, O'Leary DD (2010) Visual map development: Bidirectional signaling, bifunctional guidance molecules, and competition. *Cold Spring Harb Perspect Biol* 2(11):a001768.
- Flanagan JG (2006) Neural map specification by gradients. *Curr Opin Neurobiol* 16(1):59–66.
- Cline HT (1991) Activity-dependent plasticity in the visual systems of frogs and fish. *Trends Neurosci* 14(3):104–111.
- Feldman DE (2012) The spike-timing dependence of plasticity. *Neuron* 75(4):556–571.
- Torborg CL, Feller MB (2005) Spontaneous patterned retinal activity and the refinement of retinal projections. *Prog Neurobiol* 76(4):213–235.
- Triplett JW, et al. (2011) Competition is a driving force in topographic mapping. *Proc Natl Acad Sci USA* 108(47):19060–19065.
- Munz M, et al. (2014) Rapid Hebbian axonal remodeling mediated by visual stimulation. *Science* 344(6186):904–909.
- David SV, Vinje WE, Gallant JL (2004) Natural stimulus statistics alter the receptive field structure of v1 neurons. *J Neurosci* 24(31):6991–7006.



9. Meytlis M, Nichols Z, Nirenberg S (2012) Determining the role of correlated firing in large populations of neurons using white noise and natural scene stimuli. *Vision Res* 70:44–53.
10. Ellemberg D, Hansen BC, Johnson A (2012) The developing visual system is not optimally sensitive to the spatial statistics of natural images. *Vision Res* 67:1–7.
11. Hansen BC, Johnson AP, Ellemberg D (2012) Different spatial frequency bands selectively signal for natural image statistics in the early visual system. *J Neurophysiol* 108(8):2160–2172.
12. Gollisch T, Meister M (2008) Rapid neural coding in the retina with relative spike latencies. *Science* 319(5866):1108–1111.
13. Gaze RM, Keating MJ, Chung SH (1974) The evolution of the retinotectal map during development in *Xenopus*. *Proc R Soc Lond B Biol Sci* 185(1080):301–330.
14. Engert F, Tao HW, Zhang LI, Poo MM (2002) Moving visual stimuli rapidly induce direction sensitivity of developing tectal neurons. *Nature* 419(6906):470–475.
15. Straznicky C, Glastonbury J (1979) Anomalous ipsilateral optic fibre projection in *Xenopus* induced by larval tectal ablation. *J Embryol Exp Morphol* 50:111–122.
16. Ruthazer ES, Akerman CJ, Cline HT (2003) Control of axon branch dynamics by correlated activity in vivo. *Science* 301(5629):66–70.
17. O'Rourke NA, Fraser SE (1990) Dynamic changes in optic fiber terminal arbors lead to retinotopic map formation: An in vivo confocal microscopic study. *Neuron* 5(2):159–171.
18. Reh TA, Constantine-Paton M (1984) Retinal ganglion cell terminals change their projection sites during larval development of *Rana pipiens*. *J Neurosci* 4(2):442–457.
19. Reh TA, Constantine-Paton M (1985) Eye-specific segregation requires neural activity in three-eyed *Rana pipiens*. *J Neurosci* 5(5):1132–1143.
20. O'Rourke NA, Fraser SE (1989) Gradual appearance of a regulated retinotectal projection pattern in *Xenopus laevis*. *Dev Biol* 132(1):251–265.
21. Cline HT, Debski EA, Constantine-Paton M (1987) N-methyl-D-aspartate receptor antagonist desegregates eye-specific stripes. *Proc Natl Acad Sci USA* 84(12):4342–4345.
22. Witte S, Stier H, Cline HT (1996) In vivo observations of timecourse and distribution of morphological dynamics in *Xenopus* retinotectal axon arbors. *J Neurobiol* 31(2):219–234.
23. Olson MD, Meyer RL (1991) The effect of TTX-activity blockade and total darkness on the formation of retinotopy in the goldfish retinotectal projection. *J Comp Neurol* 303(3):412–423.
24. Ruthazer ES, Li J, Cline HT (2006) Stabilization of axon branch dynamics by synaptic maturation. *J Neurosci* 26(13):3594–3603.
25. Rajan I, Witte S, Cline HT (1999) NMDA receptor activity stabilizes presynaptic retinotectal axons and postsynaptic optic tectal cell dendrites in vivo. *J Neurobiol* 38(3):357–368.
26. Hua JY, Smith SJ (2004) Neural activity and the dynamics of central nervous system development. *Nat Neurosci* 7(4):327–332.
27. Yu X, Yoganarasimha D, Knierim JJ (2006) Backward shift of head direction tuning curves of the anterior thalamus: Comparison with CA1 place fields. *Neuron* 52(4):717–729.
28. Foster DJ, Knierim JJ (2012) Sequence learning and the role of the hippocampus in rodent navigation. *Curr Opin Neurobiol* 22(2):294–300.
29. Meister M, Berry MJ, 2nd (1999) The neural code of the retina. *Neuron* 22(3):435–450.
30. Buonomano DV, Merzenich MM (1998) Net interaction between different forms of short-term synaptic plasticity and slow-IPSPs in the hippocampus and auditory cortex. *J Neurophysiol* 80(4):1765–1774.
31. Eisner-Janowicz I, et al. (2008) Early and late changes in the distal forelimb representation of the supplementary motor area after injury to frontal motor areas in the squirrel monkey. *J Neurophysiol* 100(3):1498–1512.
32. Yoon M (1971) Reorganization of retinotectal projection following surgical operations on the optic tectum in goldfish. *Exp Neurol* 33(2):395–411.
33. Zarzecki P, et al. (1993) Synaptic mechanisms of cortical representational plasticity: Somatosensory and corticocortical EPSPs in reorganized raccoon SI cortex. *J Neurophysiol* 69(5):1422–1432.
34. Constantine-Paton M, Law MI (1978) Eye-specific termination bands in tecta of three-eyed frogs. *Science* 202(4368):639–641.
35. Katz LC, Constantine-Paton M (1988) Relationships between segregated afferents and postsynaptic neurones in the optic tectum of three-eyed frogs. *J Neurosci* 8(9):3160–3180.
36. Law MI, Constantine-Paton M (1981) Anatomy and physiology of experimentally produced striped tecta. *J Neurosci* 1(7):741–759.
37. Ide CF, Fraser SE, Meyer RL (1983) Eye dominance columns from an isogenic double-nasal frog eye. *Science* 221(4607):293–295.
38. Boss VC, Schmidt JT (1984) Activity and the formation of ocular dominance patches in dually innervated tectum of goldfish. *J Neurosci* 4(12):2891–2905.
39. Higenell V, Han SM, Feldheim DA, Scalia F, Ruthazer ES (2012) Expression patterns of Ephs and ephrins throughout retinotectal development in *Xenopus laevis*. *Dev Neurobiol* 72(4):547–563.
40. Antonini A, Stryker MP (1993) Rapid remodeling of axonal arbors in the visual cortex. *Science* 260(5115):1819–1821.
41. Darian-Smith C, Gilbert CD (1995) Topographic reorganization in the striate cortex of the adult cat and monkey is cortically mediated. *J Neurosci* 15(3 Pt 1):1631–1647.
42. Marik SA, Yamahachi H, McManus JN, Szabo G, Gilbert CD (2010) Axonal dynamics of excitatory and inhibitory neurons in somatosensory cortex. *PLoS Biol* 8(6):e1000395.
43. Campbell G, Shatz CJ (1992) Synapses formed by identified retinogeniculate axons during the segregation of eye input. *J Neurosci* 12(5):1847–1858.
44. Katz LC, Shatz CJ (1996) Synaptic activity and the construction of cortical circuits. *Science* 274(5290):1133–1138.
45. Stellwagen D, Shatz CJ (2002) An instructive role for retinal waves in the development of retinogeniculate connectivity. *Neuron* 33(3):357–367.
46. Zou DJ, Cline HT (1996) Expression of constitutively active CaMKII in target tissue modifies presynaptic axon arbor growth. *Neuron* 16(3):529–539.
47. Zou DJ, Cline HT (1999) Postsynaptic calcium/calmodulin-dependent protein kinase II is required to limit elaboration of presynaptic and postsynaptic neuronal arbors. *J Neurosci* 19(20):8909–8918.
48. McLaughlin T, Torborg CL, Feller MB, O'Leary DD (2003) Retinotopic map refinement requires spontaneous retinal waves during a brief critical period of development. *Neuron* 40(6):1147–1160.
49. Meister M, Wong RO, Baylor DA, Shatz CJ (1991) Synchronous bursts of action potentials in ganglion cells of the developing mammalian retina. *Science* 252(5008):939–943.
50. Stafford BK, Sher A, Litke AM, Feldheim DA (2009) Spatial-temporal patterns of retinal waves underlying activity-dependent refinement of retinofugal projections. *Neuron* 64(2):200–212.
51. Elstrott J, Feller MB (2010) Direction-selective ganglion cells show symmetric participation in retinal waves during development. *J Neurosci* 30(33):11197–11201.
52. Ahissar E, Arieli A (2001) Figuring space by time. *Neuron* 32(2):185–201.
53. Galimberti I, Bednarek E, Donato F, Caroni P (2010) EphA4 signaling in juveniles establishes topographic specificity of structural plasticity in the hippocampus. *Neuron* 65(5):627–642.
54. MacDonald CJ, Carrow S, Place R, Eichenbaum H (2013) Distinct hippocampal time cell sequences represent odor memories in immobilized rats. *J Neurosci* 33(36):14607–14616.
55. Howard MW, Eichenbaum H (2013) The hippocampus, time, and memory across scales. *J Exp Psychol Gen* 142(4):1211–1230.